Article:
De, A., Boudet, C. orcid.org/0009-0000-2977-1579, Nath, J. et al. (5 more authors) (2025) Electronic Hong Ou Mandel interferences to unveil the 2/3 fractional quantum Hall edge channel dynamics. Nature Communications, 16 (1). 8466. ISSN: 2041-1723

https://doi.org/10.1038/s41467-025-63308-2

nature communications

Article

https://doi.org/10.1038/s41467-025-63308-2

Electronic Hong Ou Mandel interferences to unveil the 2/3 fractional quantum Hall edge channel dynamics

Received: 11 December 2024

Accepted: 14 August 2025

Published online: 26 September 2025

Check for updates

A. De[1,4], C. Boudet[1,4], J. Nath[1], M. Kapfer[1], I. Farrer[2], D. A. Ritchie[3], P. Roulleau[1] & D. C. Glattli[1]

Electronic Hong-Ou-Mandel (HOM) current noise interferometry has revealed anyonic statistics in Fractional Quantum Hall (FQH) states at ν = 1/3 and 2/5. However, hole-conjugate phases (½ < ν < 1), like ν = 2/3, host both charge and neutral edge modes, are disorder-sensitive, and pose challenges for interferometry. We present time-domain HOM and Photon-Assisted Shot Noise (PASN) measurements at ν = 2/3 to probe edge mode dynamics and tunneling charge. Using PASN's fractional Josephson relation, we measure an e/3 tunneling charge and show that DC shot noise overestimates charge below ~100 mK. PASN reveals damping of downstream charge modes due to limited propagation of upstream neutral modes beyond a micrometer-scale equilibration length. Time-resolved HOM measurements confirm picosecond pulse broadening. These results suggest revisiting the neutral mode status, highlight the limitations of HOM interferometry in hole-conjugate phases and provide a path to explore complex FQH states that host neutral or non-Abelian modes.

Electrons confined to a plane in a strong perpendicular magnetic field form degenerate Landau levels, leading to incompressible quantum liquids. When the Landau level filling is integer or fractional, this yields the Integer or Fractional Quantum Hall Effect (IQHE[1] or FQHE[2,3]), respectively—both topological insulators with a gap and quantized Hall resistance[3]. For a filling factor $\nu = p$ integer, p Landau levels are filled and p chiral gapless co-propagating modes appear at the conductor edges, allowing a current carried by integer charges to flow. For fractional filling, the carriers are anyons carrying fractional charge[3–6] and obey fractional statistics[7–13]. Knowing how far they can maintain quantum coherence while propagating along edge channels is an important fundamental question relevant to braiding interference applications[9–16]. The answer to this question depends heavily on our understanding of how far the dynamical edge excitation can propagate along the edge with reasonable integrity for the design of practical anyon braiding experiments[9–13]. Here, we restrict ourselves to correlated states from the first Landau level, where we distinguish two types of FQHE states. The first type corresponds to filling factors $\nu = p/(2np + 1)$, $p = 1, 2, \ldots$. This is the Jain series[17] of composite fermions to which −2n quantum flux is attached to each electron, $n = 1, 2, \ldots$, which gives p co-propagating edge channels. The second type concerns the series $\nu = p/(2np\text{-}1)$, $p = 1, 2, \ldots$ were the structure of edges is more complex. For example, for $\nu = 2/3$, the ground state can be described by a hole conjugate 1/3 FQHE state[18–23]. In the absence of disorder, the edge was shown to host two counter-propagating channels[18–21] in the form of a downstream outer edge channel with conductance e^2/h, here labeled 1, and an upstream inner-edge channel with conductance $-e^2/(3h)$, labeled −1/3, leading to a conductance $4/3e^2/h$ in contradiction with the Hall conductance $2/3e^2/h$. The contradiction was resolved in a seminal paper by Kane, Fisher and Polchinski[22]. Starting from a bosonisation of the original channels in a chiral Luttinger liquid (cLL) frame[20,24], they show that the Coulomb coupling between the channels gives rise to two bosonic eigenmodes: a (quasi-)charge mode propagating downstream and a (quasi-)neutral mode propagating upstream. In a second step, they found that the addition of short-range random inter-channel tunneling, as shown in Fig. 1b, is essential to

[1]SPEC, CEA, CNRS, Université Paris-Saclay, CEA Saclay, Cedex, France. [2]School of Electrical & Electronic Engineering, University of Sheffield, Mappin Street, UK. [3]Cavendish Laboratory, University of Cambridge, J.J. Thomson Avenue, Cambridge, UK. [4]These authors contributed equally: A. De, C. Boudet. e-mail: christian.glattli@cea.fr

https://doi.org/10.1038/s41467-025-63308-2

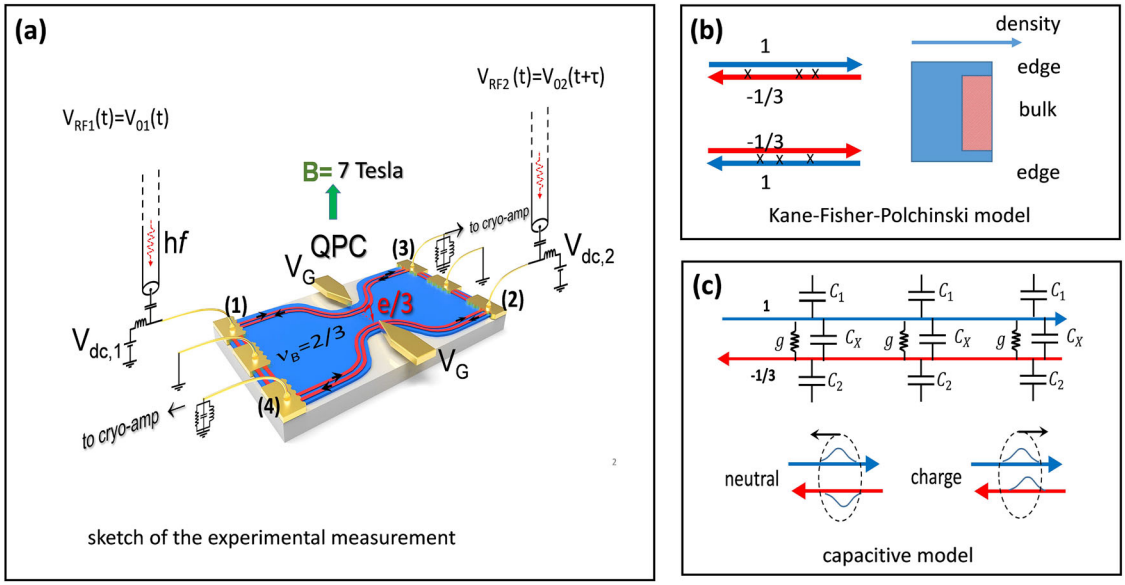

Fig. 1 | Experimental set-up and model. a Experimental principle: DC and microwave voltage can be applied to the ohmic contacts (1) and (2), injecting the current into the upper left and lower-right 2/3 edge channels. A Quantum Point Contact (QPC) weakly mixes the upper and lower inner edges, generating a Poissonian shot noise of e/3 quasiparticles, which is measured by the cross-correlation of the output currents at contacts (3) and (4). The two other contacts are grounded. When only one of the RF voltages is ON, Photo-Assisted-Shot-Noise (PASN) is measured. When both RF1 and RF2 are ON, electronic Hong Ou Mandel correlations are measured versus the time delay τ between the RF sources. **b** K-F-P model: the original counter-propagating edge channels are mixed by randomly distributed tunneling points and interaction. **c** Capacitive model[32] used here: the distributed capacitances account for the self- and inter-channel short-range interaction, the uniformly distributed tunnel conductance *g* for the random tunneling points of the K-F-P model.

restore the 2/3 conductance. The tunneling was shown to stabilize the (now fully) charged mode and the (now fully) neutral mode when the conductor length is greater than a disorder-dependent charge equilibration length $l_{eq.}$, the typical length over which an electron in the original downstream 1-channel has tunneled into the upstream "−1/3" channel. Later, by exploring further the microscopic consequence of inter-mode tunneling, further theoretical works showed that hot spots form at contact located at the downstream end of the edge channels, leading to an upstream heat flow[25–29]. As shown in ref. 30, it is likely that in some experiments the upstream heat flow plays the role naively attributed to neutral modes[31]. Indeed, modeling the dynamics of the edge modes, as done in ref. 32 and sketched in Fig. 1c, will show that the neutral modes are highly attenuated and unlikely to propagate beyond the charge equilibration length: $l_{eq.}$, typically a few microns, see Fig. S3b in the Supplementary. The non-observation of counter-propagating modes in 100 µm wide edge-channel resonators was long-noted in ref. 33. The charge mode damping was attributed to absorption in the bulk[33,34]. While in ref. 33 the >300 mK temperature lead to finite bulk conductivity, in the present work done at 20 mK, the exponentially vanishing bulk conductivity makes incoherent tunneling processes along the 2/3 edge the dominant source of damping. As they are likely to be responsible for the lack of quasiparticle interference[35,36], therefore preventing performing practical anyon braiding for the 2/3 FQHE state beyond $l_{eq.}$, it is thus of paramount importance to develop simple experimental tools on the mesoscopic scale to get information on $l_{eq.}$ whose non-universal value depends on the nature of the 2D material and its random disorder.

In this work, we use microwave excitations to unambiguously determine the tunneling quasiparticle charge e* at $\nu = 2/3$ and show that the high-frequency dynamics of the edge provide a direct way to estimate $l_{eq.}$ in a single sample. In contrast, conventional measurements using only DC excitation are problematic to perform these tasks in several respects: they can give erroneous shot noise determinations of e*, as we will demonstrate below by solving the long puzzling issue of observation of charge above e/3 at $\nu = 2/3$ at low temperature, see ref. 37.; they cannot provide direct evidence of neutral and charged modes; they cannot access the charge equilibrium length $l_{eq.}$ without using several samples of different lengths, assuming they maintain the same disorder. While the importance of investigating the dynamics of the 2/3 edge was originally suggested in the work of K-F-P[22], no high-frequency investigation was available till now on the mesoscopic scale, except the early work of ref. 33 on bulk samples which gave no information on $l_{eq.}$.

To proceed we combine microwave irradiation using photon of energy h*f* (with $k_BT/hf = 0.019$ to 0.029) and current noise measurements using a punctual scatter made with a Quantum Point Contact (QPC) to couple the opposite inner edges of the 2/3 FQHE state. The QPC is tuned in the weak backscattering regime, see schematic principle in Fig. 1a. Combining microwave irradiation and shot noise has solid advantages: − 1) the Photo-Assisted Shot Noise (PASN) provides an unambiguous metrological-like determination of the quasiparticle charge $e^* = e/3$ via the fractional Josephson relation[38–40] $e^*V = hf$, where *V* is the DC potential across the QPC and *f* is the microwave frequency. This observation assures us of the presence of the "−1/3counter-propagating inner channel and resolves the debate about the tunneling charge at $\nu = 2/3$; − 2) PASN provides information on the microwave amplitude decay along the 2/3 edge, that we can relate to the equilibration length $l_{eq.}$; − 3) sending microwave Lorentzian pulses to generate levitons on opposite sides of the QPC allows performing time-domain electronic Hong Ou Mandel (HOM) interference[41–43] from which we can attest the deformation of the pulses due to dispersive effects and exponential decay arising from the finite length $l_{eq.}$ This provides a benchmark for HOM measurements, which are central to investigating FQHE anyons.

Results and discussion

The measurements are performed on a two-dimensional electron gas made in high mobility GaAs/Ga(Al)As heterojunction with electron density $n_s = 1.11\ 10^{15}\ m^{-2}$ and zero field mobility $\mu = 300\ m^2\ V^{-1}\ s^{-1}$, see SM. The filling factor $\nu = 2/3$ occurs at field B≈7 Tesla. A sketch of the

sample with schematic external circuitry is shown in Fig. 1a. DC, low-frequency AC and microwave voltages can be applied to the ohmic contacts (1) and (2). They are used to inject a DC current or photo-excited quasiparticle-quasihole pairs towards a QPC placed at the center of the sample. Contacts (3) and (4) measure the currents transmitted and reflected by the QPC, respectively. The other two contacts are connected to ground. The sample geometry is symmetric and the distance between each ohmic contact and the central QPC is short, ~20 µm, but larger than the expected range of l_{eq}.

Identifying the nature of the inner edge at filling factor 2/3

Prior to exploring the high-frequency dynamics of the 2/3 edge, we first proceed to identify the nature of the inner-edge, expected to be a counter-propagating "−1/3 edge. This is done by a double determination of the quasiparticle charge e* tunneling between counter-propagating inner edges when they are mixed by the QPC. Two methods are used:

1) The standard method involves applying only a DC bias voltage to the injecting contact and observing the Poissonian statistics of the backscattering current noise in the WB regime. In this case, the charge e* is equal to the ratio of the current noise power to the mean backscattered current.
2) A metrological-like method based on comparing a DC bias voltage V_{DC} to microwave frequency f using the fractional Josephson relation:

$$e^* V_{DC} = \pm hf \tag{1}$$

where h is the Planck constant and V_{DC} denotes the DC voltages at which the first thermally rounded PASN singularities occur.

Method 1: The so-called DC Shot Noise (DCSN) $S_I^{DC}(V_{DC})$ is measured. It represents the increase of the noise with respect to the equilibrium noise due to the partitioning of the charges under a DC bias voltage V_{DC}. No microwave is sent to the sample, but only a DC voltage V_{DC} is applied on the upper left ohmic contact to inject the current $I_0 = (2e^2/3h)V_{DC}$ towards the QPC. For weak quasiparticles tunneling with charge e* the shot noise is given by refs. 43–45:

$$S_I^{DC}(V_{DC}, T_e) = 2e^* I_B(V_{DC})(1-R)\left(\coth\left(e^* V_{DC}/2k_B T_e\right) - 2k_B T_e/e^* V_{DC}\right) \tag{2}$$

In the large voltage limit $e^* V_{DC} \gg k_B T_e$, the charge e* is given by the ratio of $S_I^{DC}(V_{DC})$ over the backscattering current $I_B = R(V_{DC})I_0$ where $R \ll 1$ is the reflection probability. Our setup allows two choices for measuring S_I^{DC}: the Auto-Correlated Shot Noise (ACSN) $S_{I_3I_3} = S_{I_4I_4}$ of the transmitted current I_3 or the backscattering current I_4, or the Cross-Correlated Shot Noise (CCSN) $-S_{I_4I_3}$. Both measurements should provide the same information as one expects $S_{I_3I_3}(V_{DC}, T_e) = S_{I_3I_3}(0, T_e) + S_I^{DC}(V_{DC}, T_e)$ and $-S_{I_3I_4} = S_I^{DC}(V_{DC}, T_e)$ as long as $S_{I_3I_3}(0, T_e)$, proportional to the electronic temperature T_e, remains constant. Up to now, most fractional charge determinations at 2/3 were done using the ACSN, see ref. 37. However, the latter may significantly overestimate e* due to electron heating. Indeed, inelastic charge equilibration processes between the 1 and −1/3 channel at 2/3 give an electronic temperature $T_e \propto V_{DC}$ originating from "hot spots discussed in ref. 25,26,30, which increases the ACSN. In contrast, the CCSN gives a fair determination of e* as heating effects give only a weak underestimation, see Supplementary Note B for a discussion on ACSN and CCSN.

The ACSN and CCSN measurements are shown in Fig. 2A. For ACSN, the $V_{DC} = 0$ shot noise has been subtracted for better comparison with CCSN. The upper graph shows that the ACSNs $S_{I_3I_3}$ and $S_{I_4I_4}$ measured at 16 mK versus the DC voltage are well above the CCSN $S_{I_3I_4}$. The red dashed curve is Eq. (2) using e*=e/3 and I_B calculated from the simultaneously measured reflection $R(V_{DC})$ shows good agreement with the CCSN. In contrast, if only ACSN were measured, the charge e* would have been overestimated. The figure below shows similar measurements done at a higher temperature, 110 mK. We observe that ACSN and CCSN merge together, and both measurements provide a correct determination of e*. The bottom graph of panel (A) shows how e* deduced from ACSN and CCSN varies with temperature. As discussed in the Supplementary, we find the variations are consistent with an electronic temperature varying as $T_e(V) = \sqrt{T^2 + \left(\frac{\lambda e V_{DC}}{k_B}\right)^2}$ with $\lambda \approx 0.05$. λ is a non-universal phenomenological parameter that accounts for the Wiedemann–Franz law, which describes the balance between the heat generated by the finite current in the input channel and the finite electronic thermal conductivity. From now on, all current noise measurements presented here will use cross-correlations, which are much more reliable. We note that a recent study (ref. 46) observed the signature of 'hot spots' in noise measurements at $\nu = 2/3$, and advocated the use of CCSN measurements at low temperatures. However, no detailed comparison was made between ACSN and CCSN.

Method 2: In a second step, we superimpose on the injecting contact a microwave voltage of amplitude $V_0\cos(2\pi f t)$ to the DC voltage V_{DC}. This generates a photo-assisted shot noise, or PASN, predicted to be refs. 47–50:

$$S_I^{PASN}(V_{DC}) = \sum_{l=-\infty}^{+\infty} J_l^2\left(\frac{e^* V_{ac}}{hf}\right) S_I^{DC}\left(V_{DC} + \frac{lhf}{e^*}\right) \tag{3}$$

This Tien–Gordon-like expression is very useful because, knowing the experimental DCSN $S_I^{DC}(V_{DC})$ we can predict the PASN from the photo-absorption probabilities $J_l^2(\frac{e^* V_{ac}}{hf})$. Here, J_l is an integer Bessel function, and V_{ac} is the microwave excitation voltage at the QPC. Furthermore, the thermally rounded zero-bias singularity of the DCSN is replicated when V_{DC} is a multiple of the voltage hf/e*, which is a fractional Josephson relation[38]. This provides a metrological way to determine e*, a method already used to determine the e/3 and e/5 tunneling charges at $\nu = 2/5$ in ref. 39.

Figure 2B shows our experimental PASN measurements used to determine e*. The upper left and right graphs show cross-correlation DCSN (black open circles) and PASN (blue open circles) measurements for microwave frequencies 22 and 17 GHz, respectively. For better reliability, DCSN and PASN measurements are obtained from the CCSN $-S_{I_3I_4}$. The red dashed curves are best PASN fits from Eq. (3) with e* = e/3 and V_{ac} = 170 µV and 180 µV, respectively. Although the fits are sufficient to confirm that e* = e/3, in order to better visualize the "Josephsonvoltages $\pm hf/e^*$, we construct the excess PASN (XSPASN) from which the zero-photon absorption/emission part is subtracted:

$$S_I^{XSPASN}(V_{DC}) = \sum_{|l|\geq 1}^{+\infty} J_l^2\left(\frac{e^* V_{ac}}{hf}\right) S_I^{DC}\left(V_{DC} + \frac{lhf}{e^*}\right) \tag{4}$$

The XSPASN graphs for 22 GHz and 17 GHz are displayed below their respective PASN graphs. Local XSPASN minima give the loci of the "Josephson voltage associated with charge e*=e/3. The lower left graph shows a similar XSPASN curve for a lower microwave frequency of 14.15 GHz. All XSPASN curves are rescaled in the lower-right figure, with $e^* V_{DC}/hf$ used as the x axis.

In a recent theoretical work[51], the simultaneous tunneling of anyon of charge e/3 and 2e/3 is considered. The authors showed that even a few % relative amount of 2e/3 tunneling charge can be observable as a secondary XSPASN minima at voltages $\pm 3hf/2e$ in addition to the main $\pm 3hf/e$ minima. Within our experimental noise uncertainty, no 2e/3 charge tunneling is detectable.

https://doi.org/10.1038/s41467-025-63308-2

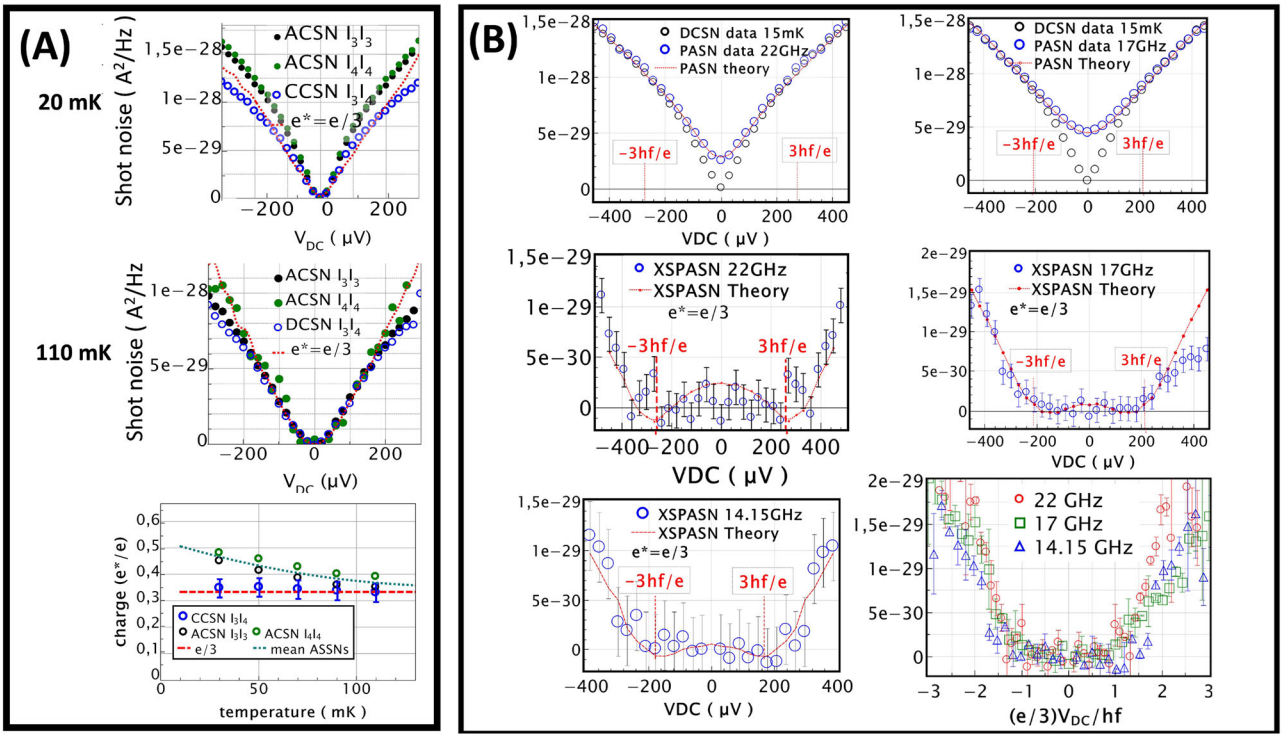

Fig. 2 | determination of e*. A ACSN (black and green open circle) and CCSN (open blue circles) measured at 16 mK (top graph) and 100 mk (middle graph). The bottom graph shows the apparent evolution of e* measured by ACSN (black and green open circles) and CCSN (blue circles) versus temperature. The dashed line denotes e* = e/3, and the green dashed line is a guide for ACSN variations. **B** DCSN (open black circles) and PASN (blue circles) measured for 22 (left) and 17 GHz (right) microwave excitation (V_{ac} = 170 and 180 μV). The red dashed curves are fits using Eq. (4) and electronic temperature T_e = 75 and 110 mK, respectively. The middle graphs show the corresponding XSPASN for 22 (left) and 17 GHz (right). The minima are found close to the 'Josephson' voltages of 272 μV and 210 μV, respectively. For the lowest frequencies, the minima are found to be slightly shifted to a lower value both theoretically and experimentally due to thermal rounding and non-linear IVC. The graph in the bottom left corner shows XSPASN for 14.15 GHz. The bottom right figure plots all XSPASN curves versus voltage in units of 3hf/e on the *x* axis. Error bars in each figure correspond to the residual Gaussian statistical noise originating from the cryogenic amplifier noise after time-averaging.

To conclude this part, method 2 provides an unambiguous determination of an e/3 tunneling charge at 2/3 and, within our uncertainty, eliminates the possibility of a few % concomitant tunneling of charge 2e/3. Method 1 resolves the puzzling larger e* values previously observed at low temperatures due to the use of ACSN measurements alone. The electron heating model presented in the Supplementary Part B provides a rational explanation for the artefacts of DC shot noise charge measurements at 2/3.

2/3 edge-channel dynamic model

Now that we have identify e* and therefore the fractional nature of the inner edge, we can address the dynamics of the 2/3 edge. As a guide, we use the incoherent inter-channel tunneling model developed in refs. 25–29. characterized by a constant distributed tunneling conductance $g = \frac{e^2}{2h l_{eq.}}$ of electrons between the 1 outer channel and the −1/3 edge channel. In the Luttinger Liquid (LL) approach, the tunneling element g is expected to depend on the difference between the local electrochemical potentials of the inner and outer edge states. However, when the microwave voltage amplitude applied to the injecting Ohmic contacts is small, specifically $V_0 \ll 2\pi k_B T_e/e$ (where T_e is the electronic temperature), we can approximate *g* as a phenomenological constant. To describe the edge dynamics, we follow ref. 32. which solves the collective modes of the 2/3 edge in a transmission line model. Instead of considering the inter-mode coupling and the intra-mode interaction as phenomenological parameters as done in standard cLL models, ref. 32. uses realistic parameters where the interaction can be modeled by capacitances[32,52–54] see Fig. 1c. The equation of motion of the current can be written as follows:

$$\frac{\partial}{\partial t}\vec{\boldsymbol{I}} = -\boldsymbol{\sigma C^{-1}}\frac{\partial}{\partial x}\vec{\boldsymbol{I}} - -\boldsymbol{\sigma C^{-1} g \sigma^{-1}}\vec{\boldsymbol{I}} \tag{5}$$

where $\vec{\boldsymbol{I}} = \begin{pmatrix} I_1 \\ I_2 \end{pmatrix}$, with $I_{1(2)}(x,t)$ denoting the current in outer (inner) channel at time *t* and point *x*, $\boldsymbol{\sigma} = \sigma_q \begin{pmatrix} 1 & 0 \\ 0 & -1/3 \end{pmatrix}$ accounts for the channel conductance with $\sigma_q = e^2/h$, $\boldsymbol{g} = g\begin{pmatrix} 1 & -1 \\ -1 & 1 \end{pmatrix}$ describes the inter-channel tunneling conductance and $\boldsymbol{C} = \begin{pmatrix} C_1 + C_X & -C_X \\ -C_X & C_2 + C_X \end{pmatrix}$ the interaction, with $C_{1(2)}$ the outer (inner) channel self-capacitance per unit length and C_X the inter-channel capacitance per unit length. In the absence of inter-channel conductance, Eq. (1) is equivalent to that used in the K-F-P model for cLL bosonization (see SM). In the following, we will use realistic parameters with $C_1 = C_2 =$ 0.1 nF/m and $C_X =$ 0.4nF/m as in ref. 32. Variations around these parameter values do not qualitatively change the predictions. Here, we used geometric capacitances in Eq. (1) instead of electrochemical capacitances $\tilde{C}_{1(2)}$ as, in GaAs 2DEG, we can safely neglect the contribution of quantum capacitances $c_{q,1(2)}$, with $\frac{1}{\tilde{C}_{1(2)}} = \frac{1}{C_{1(2)}} + \frac{1}{c_{q,1(2)}}$. This would not be the case for Graphene 2DEGs for which the high Fermi velocity leads to a non-negligible quantum capacitance contribution.

Equation(5) describes the propagation of the coupled modes with possible decay due to the tunneling conductance. We seek a solution

https://doi.org/10.1038/s41467-025-63308-2

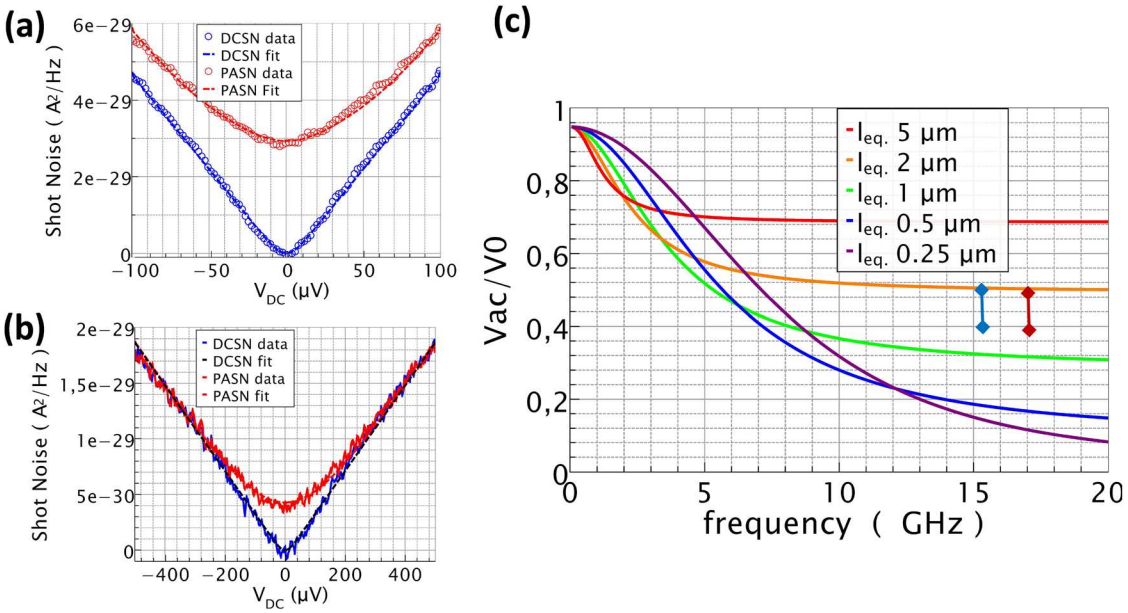

Fig. 3 | Measuring de charge mode attenuation on the 2/3 fractional edge. **a**, **b** show DCSN and PASN measurements using $f = 15.3$ GHz microwave excitation on contact (1) versus DC bias voltage. **a** $\nu = 2$: inner edge weakly backscattered, transmission $D = 0.96 \pm 1\%$. The graph shows the experimental cross-correlated DCSN and PASN amplitude versus DC voltage (blue and red circles, respectively). The blue and red dashed curves are fits based on Eq. (2) and Eq. (3) for DCSN and PASN with $e^* = e$ and, respectively $T_e = 31.0 \pm 1.5$ mK and 95 ± 5 mK. Equation(4) gives $V_{ac}(\nu = 2) = 70.1 \pm 3$ μV ($e^* = e$) for −6 dBm rf source power; **b** $\nu = 2/3$: inner-edge transmission 0.98. DCSN and PASN data are taken for double V_{ac} microwave amplitude (+6 dBm rf source power) to compensate for the lower tunneling charge $e^* = e/3$. The DCSN and PASN fits give, respectively $T_e = 29 \pm 1.5$ mK and 183 ± 9 mK and $V_{ac}(\nu = 2/3) = 143 \pm 3$ μV for; **c** charge mode amplitude reduction V_{ac}/V_0 expected for $\nu = 2/3$ after the 20 μm contact-to-QPC propagation length and calculated for various $l_{eq.}$ using the model given by Eq. (5). The short blue vertical line corresponds to the range of the V_{ac} ($\nu = 2/3$, +6 dBm) reduction found between 0.50 and 0.41 for the present 15.3 GHz drive. The red vertical segment is the reduction between 0.48 and 0.40 found at 17.05 GHz, see SM. We estimate 1 μm $\leq l_{eq.} \leq$ 2μm.

of the form $\begin{pmatrix} I_1(x,t) \\ I_2(x,t) \end{pmatrix} = \begin{pmatrix} I_1 \\ I_2 \end{pmatrix} \exp i(kx - \omega t)$. The local electrochemical potential expressed in units of voltage are related to the local current via $V_1(x,t) = I_1(x,t)/\sigma_q$ and $V_2(x,t) = -3I_2(x,t)/\sigma_q$. The diagonalization of (5) gives two eigenmodes labeled (I) and (II). Solution (I) corresponds to a downstream mode, i.e. with $\mathrm{Real}\left(k_{(I)}\right) = k'_{(I)} > 0$ and weak decay $\mathrm{Im}\left(k_{(I)}\right) = k''_{(I)} 0$. The mode is close to a charge mode with the inner and outer channel voltages almost in phase, i.e. $V_1(x,t) \cong V_2(x,t)$. Solution (II) correspond to an upstream mode, i.e. with $\mathrm{Real}\left(k_{(II)}\right) = k'_{(II)} < 0$ and strong decay $\mathrm{Im}\left(k_{(II)}\right) = k''_{(II)} < 0$. The mode is almost neutral $V_1(x,t) \cong -V_2(x,t)$ with inner and outer voltage almost out of phase. The decay lengths $1/k''_{(I),(II)}$ "or each mode are plotted in Figs. S4b and S5b of the Supplementary. Because the outer and inner channel voltages are out of phase, a large inter-edge tunnel current leads to a strong attenuation of the neutral mode. Indeed, we find $\frac{1}{k''_{(II)}} < l_{eq.}$ at all frequencies. Consequently, the K-F-P neutral modes cannot propagate beyond the charge equilibration length. In the seminal work of K-F-P the charge mode dynamics were considered, but the extremely strong decay of neutral modes was not discussed. As recently shown in ref. 30., it is likely that their role has been overestimated in the previous literature[31]. In contrast, mode (I), having in-phase inner and outer channel voltages, is associated with little inter-channel tunneling, leading to large distance propagation. An important parameter is the cross-over frequency:

$$f_{C.O.} = \frac{1}{2\pi} \frac{e^2}{2hC_X l_{eq.}} \cong \frac{7.7GHz}{l_{eq.}[\mu m]} \quad (6)$$

For $f \ll f_{C.O.}$, the inter-channel coupling is dominated by tunneling, and one can neglect the Coulomb coupling, while for $f \gg f_{C.O.}$ interaction dominates and tunneling is negligible. For frequency in the vicinity of $f_{C.O.}$ one expects important changes in the frequency response of the 2/3 edge. We anticipate dispersive effects that will alter the shape of the charge pulse, which can be investigated using HOM shot noise measurements. This is shown in Fig. S4a, where the computed phase velocity of the charge mode is plotted versus frequency. We also expect strong variations of the frequency-dependent attenuation of the charge mode, also affecting charge pulse propagation, see Fig. 3c in the main text and S4(b) in the SM.

PASN measurements

We first present PASN measurements to probe the quasiparticle of the inner "-1/3" channel and estimate the charge mode attenuation. Then we will show the results of electronic HOM shot noise measurements.

Figure3 shows PASN measurements done at $\nu = 2$ and $\nu = 2/3$ at microwave frequency $f = 15.3$ GHz. Comparing the V_{ac} amplitudes deduced from the PASN fits of Fig. 3a, b the attenuation $V_{ac}(\nu = 2/3)/V_0$ at $\nu = 2/3$ can be estimated ranging between 0.5 and 0.41, respectively, assuming no or, more likely, 10% charge mode attenuation at $\nu = 2$. Figure 3c shows the expected attenuation versus frequency computed from the solutions of Eq. (5) for various l_{eq}. The range of attenuation measured at 15.3 GHz is indicated by the blue vertical segment. Similar measurements taken at 17.05 GHz are indicated by a red segment, see Supplementary Note D1. Comparing our data with the model provides an estimation of the charge equilibration length 1 μm $\leq l_{eq.} \leq$ 2 μm. The present estimation is reasonable as it is found to be weakly dependent on the actual value of the coupling capacitance, C_X, which may vary depending on how sharply the 2DEG is confined laterally.

https://doi.org/10.1038/s41467-025-63308-2

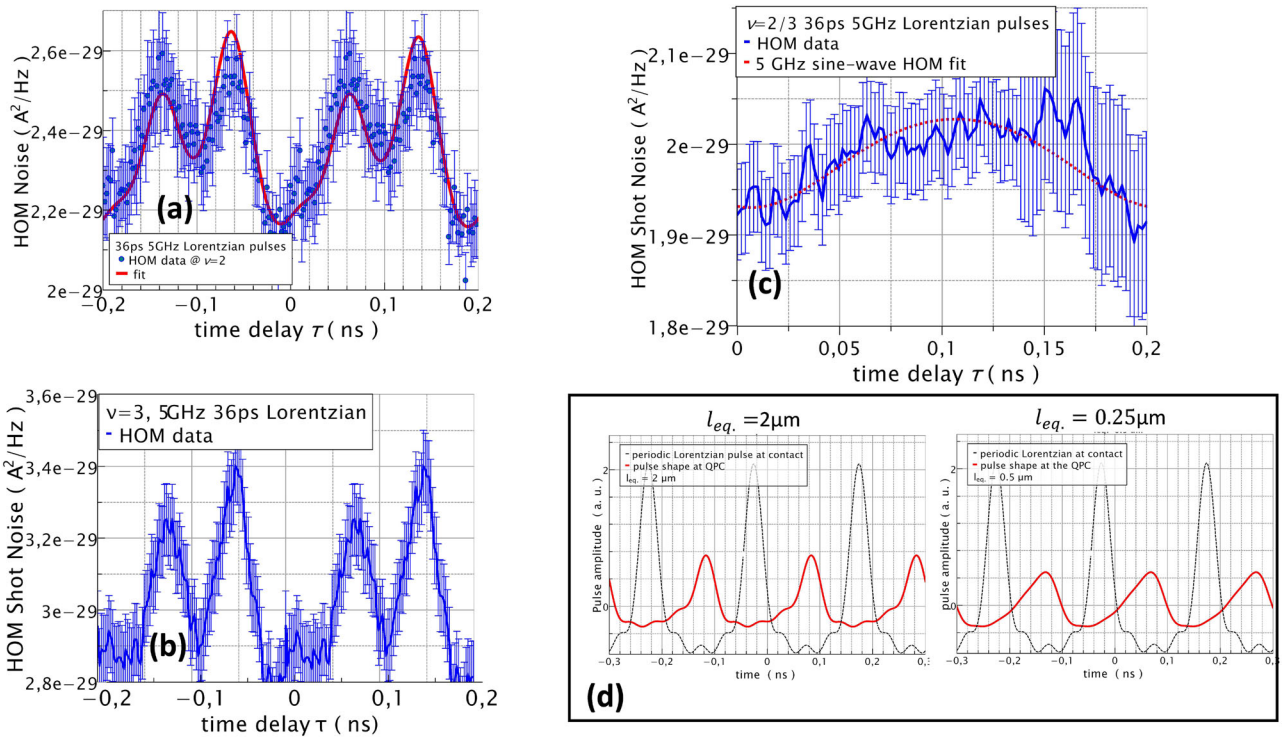

Fig. 4 | Hong Ou Mandel interference of the e/3 anyons of the $\nu = 2/3$ edge channel. Lorentzian pulses of 36 ps full width at mid-height are periodically injected at 5 GHz repetition frequency on opposite contacts with a relative time delay τ and the cross-correlated noise is measured. **a** Absolute value of the negative HOM cross-correlated noise versus time delay at filling factor $\nu = 2$. To better appreciate the variations, the data taken for $0 < \tau < 0.2$ ns have been replicated by a negative shift of one period. Multiple dips within the single period ($T = 0.2$ ns) can be described by split, undeformed Lorentzian pulses. (red dashed line fit) according to refs. 49,50. The fit uses four $\Delta_{i,j}$: τ–20 ps, τ-97 ps, τ–150 ps, τ–27 ps, known modulo 200 ps, see Supplementary Note D2. **b** same for ν = 3. **c** HOM noise of the e/3 fractional excitations observed at $\nu = 2/3$. The absence of narrow dips and a single broad variation against τ confirms the small $l_{eq.}$ and the dispersive effect predicted by the model. The red dashed curve is a tentative HOM noise fit where the deformed pulses have been approximated to a 5 GHz sine-wave. **d** computed pulse deformation (red curves) for 20 μm propagation length and $l_{eq.}$ = 2 μm (left graph) and 0.25 μm (right graph). Note the absence of neutral mode because of strong decay. As a reference, the black dashed curves correspond to the Lorentzian voltage pulse injected on the ohmic contact before propagation. Error bars in each figure correspond to the residual Gaussian statistical noise originating from cryogenic amplifier noise after time-averaging.

Electronic Hong Ou Mandel measurements

Here, the goal is to further probe the above model by checking for the expected deformation of narrow charge pulses due to inter-channel tunneling between counter-propagating edge channel at $\nu = 2/3$. The reason for pulse shape deformation is twofold. Figure 3c shows that, at $\nu = 2/3$, the attenuation of the charge mode is stronger at a large frequency than at a lower frequency. Thus, cutting the high-frequency components is likely to broaden narrow pulses. Another reason is the dispersive effect arising from the charge pulse phase velocity, which shows a pronounced variation for a wide frequency range around the cross-over frequency $f_{C.O.} = \frac{1}{2\pi}\frac{e^2}{2\hbar C_\chi l_{eq}}$, see Fig S4a in the Supplementary. In contrast, for $\nu = 2$ or 3, co-propagating channels and rare inter-channel tunneling mixing points are expected to preserve the overall shape of narrow pulses while they propagate along the 20 μm long distance from the injecting contact to the QPC.

To proceed, we generate periodic Lorentzian pulses with 5 GHz repetition frequency. This is done using an RF-source generating the four first harmonics, coherent in phase and exponentially decreasing in amplitude, whose sum accurately approximates Lorentzian pulses with tunable width[55–57], namely 36 ps and 72 ps, see SM.

We first perform the HOM shot noise experiment at integer filling factors $\nu = 2$ and 3, see Fig. 4a, b, respectively. This provides a convenient benchmarking of the quality of the pulse sent on the sample, as we do not expect significant deformation along integer edges. Indeed the measurements show clear HOM dips whose width at half amplitude is consistent with a doubling of the 36 ps width (as HOM variation can be viewed as a kind of pulse convolution, see Supplementary Note D2 and HOM measurements in ref. 56). We note however that the periodic HOM noise variation, with period $1/f = 200$ ps does not show a single HOM dip centered at time delay τ = 0 but a weaker replica around τ = 95 ps. The origin of the multiple HOM dips has been discussed in ref. 58,59 and attributed to a few discrete inter-channel tunnel mixing points. For a unique mixing point localized between the injecting contact and the QPC in each input channel, the general expression is of the form $Cst + AS_{HOM}(\Delta_{13}) + BS_{HOM}(\Delta_{23}) + CS_{HOM}(\Delta_{14}) + DS_{HOM}(\Delta_{24})$ where $S_{HOM}(.)$ is the generic HOM noise of two colliding Lorentzian pulses and $\Delta_{i,j}$ denotes various propagation time-delays. The pre-factors (A-D) are related to the QPC transmission and the tunneling point mixing amplitudes in each input arms, see Supplementary Note D2. In Fig. 4a, we show the measured HOM noise and a fit using the previous form. This confirms that the HOM dips are not broadened but simply duplicated as predicted in refs. 58,59. A detailed study at $\nu = 2$, will be published elsewhere[51]. Similar features are shown in Fig. 4b for $\nu = 3$ for which discrete mixing points are also expected to lead to multiple HOM dips. Figure 4c shows the HOM noise at ν = 2/3. In contrast to Fig. 4a, b no narrow HOM dips are observable but only an asymmetric broad variation versus the time delay τ. Indeed, Fig. 4d shows the simulation of the shape of Lorentzian pulses injected at the ohmic contact (black dashed curve) and after their propagation along the 2/3 edge towards the QPC over the 20 μm length. The curves are computed for $l_{eq.}$ = 2 μm (left) and 0.25 μm (right). They show increasing broadening and deformation for smaller $l_{eq.}$ as expected from high-frequency attenuation and dispersive effects.

In summary, exploiting microwave photo-assisted shot noise, our measurements provide the unambiguous determination of the tunneling charge at filling factor 2/3, while showing that DC shot noise approaches are unable to provide reliable e* determination at 2/3, solving the long-standing puzzle of e* increasing above e/3 at low temperatures. Microwave photo-assisted shot noise and two-particle dynamical interferometry offer insights into the charge dynamics of the ν = 2/3 edge at a mesoscopic scale. They also provide a practical estimate of the charge equilibration length $l_{eq.}$, beyond which anyon braiding interferometry is likely to be unfeasible. Our findings align with models predicting that K-F-P neutral modes cannot propagate beyond $l_{eq.}$ prompting a reevaluation of the role of neutral modes in previous experimental studies where $l_{eq.}$ is significantly shorter than the relevant sample dimensions. Our approach is versatile and can be applied to a variety of quantum Hall phases exhibiting counter-propagating edge or interface[60] modes, including those hosting non-Abelian anyons, as well as to other topological 2D materials at various filling factors.

Methods

Experiments are done in a Cryoconcept dry dilution refrigerator with a 20 mK base temperature equipped with a 14.5 T dry superconducting magnet. Conductance measurements are done using lock-in amplifiers at 270 Hz frequency and 2 μV excitation voltage. Noise measurements are made using homemade cryogenic amplifiers and followed by fast digital acquisition using an ADLINK PCIe-9852 card, providing real-time acquisition. The low-frequency noise spectrum is obtained by FFT computation using a PC computer. The two microwave voltages are generated by an APMS20G-4-ULN Anapico rf source, followed by 60dB cryogenic attenuators distributed along the low-temperature coaxial lines of the cryostat.

Data availability

All data, code, and materials used in the analysis are available upon request in some form to any researcher for purposes of reproducing or extending the analysis. The figure data files are available at Zenodo repository https://zenodo.org/records/16745945.

References

1. Klitzing, K. V., Dorda, G. & Pepper, M. New method for high-accuracy determination of the fine-structure constant based on quantized Hall resistance. *Phys. Rev. Lett.* **45**, 494 (1980).
2. Tsui, D. C., Stormer, H. L. & Gossard, A. C. Two-dimensional magnetotransport in the extreme quantum limit. *Phys. Rev. Lett.* **48**, 1559 (1982).
3. Laughlin, R. B. Anomalous quantum Hall effect: an incompressible quantum fluid with fractionally charged excitations. *Phys. Rev. Lett.* **50**, 1395 (1983).
4. Saminadayar, L., Glattli, D. C., Jin, Y. & Etienne, B. Observation of the e/3 fractionally charged Laughlin quasiparticles. *Phys. Rev. Lett.* **79**, 2526–2529 (1997).
5. de-Picciotto, R. et al. Direct observation of a fractional charge. *Nature* **389**, 162–164 (1997).
6. Reznikov, M., de Picciotto, R., Griffiths, T. G., Heiblum, M. & Umansky, V. Observation of quasiparticles with one-fifth of an electron's charge. *Nature* **399**, 238 (1999).
7. Arovas, D., Schrieffer, J. & Wilczek, F. Fractional statistics and the quantum Hall effect. *Phys. Rev. Lett.* **53**, 722–725 (1984).
8. Halperin, B. I. Statistics of quasiparticles and the hierarchy of fractional quantized Hall states. *Phys. Rev. Lett.* **52**, 1583–1586 (1984).
9. Nakamura, J., Liang, S., Gardner, G. C. & Manfra, M. J. Direct observation of anyonic braiding statistics. *Nat. Phys.* **16**, 931–936 (2020).
10. Bartolomei, H. et al. Fractional statistics in anyon collisions. *Science* **368**, 173–177 (2020).
11. Glidic, P. et al. Cross-correlation investigation of Anyon statistics in the ν=1/3 and and ν=2/5 and fractional quantum Hall states. *Phys. Rev. X* **13**, 011030 (2023).
12. Ruelle, M. et al. Comparing fractional quantum Hall laughlin and jain topological orders with the Anyon collider. *Phys. Rev. X* **13**, 011031 (2023).
13. Nakamura, J., Liang, S., Gardner, G. C. & Manfra, M. J. Fabry-Pérot interferometry at the ν=2/5 fractional Quantum Hall state. *Phys. Rev. X* **13**, 041012 (2023).
14. Rosenow, B., Levkivskyi, I. P. & Halperin, B. I. Current correlations from a mesoscopic Anyon collider. *Phys. Rev. Lett.* **116**, 156802 (2016).
15. Han, C., Park, J., Gefen, Y. & Sim, H.-S. Topological vacuum bubbles by Anyon braiding. *Nat. Commun.* **7**, 11131 (2016).
16. Jonckheere, T., Rech, J., Grémaud, B. & Martin, T. Anyonic statistics revealed by the Hong-Ou-Mandel dip for fractional excitations. *Phys. Rev. Lett.* **130**, 186203 (2023).
17. Jain, J. K. Composite-fermion approach for the fractional quantum Hall effect. *Phys. Rev. Lett.* **63**, 199 (1990)
18. MacDonald, A. H. Edge states in the fractional-quantum-Hall-effect regime. *Phys. Rev. Lett.* **64**, 222 (1990).
19. Johnson, M. D. & MacDonald, A. H. Composite edges in the ν=2/3 fractional quantum Hall effect. *Phys. Rev. Lett.* **67**, 2060 (1991).
20. Wen, X. G. Electrodynamical properties of gapless edge excitations in the fractional quantum Hall states. *Phys. Rev. Lett.* **64**, 2206 (1990).
21. Meir, Y. Composite edge states in the ν=2/3 fractional quantum Hall regime. *Phys. Rev. Lett.* **72**, 2624 (1994).
22. Kane, C. L., Fisher, M. P. A. & Polchinski, J. Randomness at the edge: theory of quantum Hall transport at filling ν=2/3. *Phys. Rev. Lett.* **72**, 4129 (1994).
23. Wang, J., Meir, Y. & Gefen, Y. Edge reconstruction in the ν=2/3 Fractional Quantum Hall State. *Phys. Rev. Lett.* **111**, 246803 (2013).
24. Wen, X. G. Gapless boundary excitations in the quantum Hall states and in the chiral spin states. *Phys. Rev. B* **43**, 11025 (1991).
25. Nosiglia, C., Park, J., Rosenow, B. & Gefen, Y. Incoherent transport on the *ν*=2/3 quantum Hall edge. *Phys. Rev. B* **98**, 115408 (2018).
26. Park, J., Mirlin, A. D., Rosenow, B. & Gefen, Y. Noise on complex quantum Hall edges: chiral anomaly and heat diffusion. *Phys. Rev. B* **99**, 161302 (2019).
27. Spanslätt, C., Park, J., Gefen, Y. & Mirlin, A. D. Conductance plateaus and shot noise in fractional quantum Hall point contacts. *Phys. Rev. B* **101**, 075308 (2020).
28. Sourav, M., Ankur, D., Yuval, G. & Moshe, G. Shot noise as a diagnostic in the ν=2/3 fractional quantum Hall edge zoo. arXiv:2307.05175v3 (2024).
29. Sourav, M. & Ankur, D Experimentally motivated order of length scales affect shot noise. arXiv:2307.08264 (2023).
30. Glattli, D. C., Boudet, C., De, A. & Roulleau, P A Toy model for the 2/3 fractional quantum Hall edge channel, arXiv:2407.07208, *Phys. Rev. Res.* (2024).
31. Bid, A. et al. Observation of neutral modes in the fractional quantum Hall regime. *Nature* **466**, 585 (2010).
32. Fujisawa, T. & Lin, C. Plasmon modes of coupled quantum Hall edge channels in the presence of disorder-induced tunneling. *Phys. Rev. B* **103**, 165302 (2021).
33. Ashoori, R. C., Stormer, H. L., Pfeiffer, L. N., Baldwin, K. W. & West, K. Edge magnetoplasmons in the time domain. *Phys. Rev. B* **45**, 3894 (1992).
34. Kumada, N. et al. Resonant edge magnetoplasmons and their decay in graphene. *Phys. Rev. Lett.* **113**, 266601 (2014).
35. Goldstein, M. & Gefen, Y. Suppression of Interference in Quantum Hall Mach-Zehnder geometry by upstream neutral modes. *Phys. Rev. Lett.* **117**, 276804 (2016).

36. Bhattacharyya, R., Mitali, B., Heiblum, M., Mahalu, D. & Umansky, V. Melting of interference in the fractional quantum Hall effect: appearance of neutral modes. *Phys. Rev. Lett.* **122**, 246801 (2019).
37. Bid, A., Ofek, N., Heiblum, M., Umansky, V. & Mahalu, D. Shot noise and charge at the 2/3 composite fractional quantum Hall state. *Phys. Rev. Lett.* **103**, 236802 (2009).
38. Wen, X. G. Edge transport properties of the fractional quantum Hall states and weak-impurity scattering of a one-dimensional charge-density wave. *Phys. Rev. B* **44**, 5708–5719 (1991).
39. Kapfer, M. et al. A Josephson relation for fractionally charged anyons. *Science* **363**, 846–849 (2019).
40. Bisognin, R. et al. Microwave photons emitted by fractionally charged quasiparticles. *Nat. Commun.* **10**, 1708 (2019).
41. Bocquillon, E. et al. Coherence and Indistinguishability of Single Electrons Emitted by Independent Sources. *Science* **339**, 1054–1057 (2013).
42. Jullien, T. et al. Quantum tomography of an electron. *Nature* **514**, 603–607 (2014).
43. Taktak, I. et al. Two-particle time-domain interferometry in the Fractional Quantum Hall Effect regime. *Nat. Commun.* **13**, 5863 (2022).
44. Kane, C. L. & Fisher, M. P. Nonequilibrium noise and fractional charge in the quantum Hall effect. *Phys. Rev. Lett.* **72**, 724 (1994).
45. Fendley, P., Ludwig, A. W. & Saleur, H. Exact nonequilibrium dc shot noise in luttinger liquids and fractional quantum hall device. *Phys. Rev. Lett.* **75**, 2196 (1995).
46. Veillon, A. et al. Observation of the scaling dimension of fractional quantum Hall anyons. *Nature* **632**, 517 (2024).
47. Crépieux, A., Devillard, P. & Martin, T. Photoassisted current and shot noise in the fractional quantum Hall effect. *Phys. Rev. B* **69**, 205302 (2004).
48. Lesovik, G. & Levitov, B. L. S. Noise in an ac biased junction: nonstationary Aharonov-Bohm effect. *Phys. Rev. Lett.* **72**, 538–541 (1994).
49. Pedersen, M. & Büttiker, H. M., Scattering theory of photon-assisted electron transport. *Phys. Rev. B* **58**, 12993 (1998).
50. Safi, I. Time-dependent transport in arbitrary extended driven tunnel junctions. *arXiv* https://arxiv.org/abs/1401.5950 (2014).
51. Iyer, K. et al. Photo-assisted shot noise probes multiple charge carriers in quantum Hall edges. *Phys. Rev. B* **111**, 245433 (2025).
52. Hashisaka, M. & Fujisawa, T. Tomonaga–Luttinger-liquid nature of edge excitations in integer quantum Hall edge channels T. *Rev. Phys.* **3**, 32 (2018).
53. Hashisaka, M. et al. Distributed-element circuit model of edge magnetoplasmon transport. *Phys. Rev. B* **88**, 235409 (2013).
54. Kamata, H., Irie, H., Sasaki, S., Kumada, N. & Muraki, K. Time-resolved counterpropagating edge transport in the topological insulating phase. *Phys. Rev. Res.* **6**, 043073 (2024).
55. Aluffi, M. et al. Ultrashort electron wave packets via frequency-comb synthesis. *Phys. Rev. Appl.* **20**, 034005 (2023).
56. Dubois, J. et al. Minimal-excitation states for electron quantum optics using levitons. *Nature* **502**, 659 (2013).
57. Assouline, A. et al. Emission and coherent control of levitons in graphene. *Science* **382**, 1260–1264 (2023).
58. Acciai, M., Roulleau, P., Taktak, I., Glattli, D. C. & Splettstoesser, J. Influence of channel mixing in fermionic Hong-Ou-Mandel experiments. *Phys. Rev. B* **105**, 125415 (2022).
59. Acciai, M., Roulleau, P., Glattli, D. C. & Splettstoesser, J. Impact of channel mixing on the visibility of two-particle interferometry in quantum Hall edge states. *JPS Conf. Proc.* **38**, 011174 (2023).
60. Hashisaka, M. et al. Coherent-incoherent crossover of charge and neutral mode transport as evidence for the disorder-dominated fractional edge phase. *Phys. Rev. X* **13**, 031024 (2023).

Acknowledgements

The authors acknowledge financial support from the European H2020 FET-OPEN UltraFastNano #862683 Grant (A.D., J.N., P.R., D.C.G.). We thank P. Jacques and Hervé Hermange for technical help, and we acknowledge discussions with M. Acciai, J. Splettstoesser, Y. Gefen, M. Goldstein, A. Das, S. Manna, J. Rech, and Th. Jonkheere, Th. Martin, and members of the Saclay Nanoelectronics team.

Author contributions

D.C.G. designed and supervised the project. mlC.B. & A.D. equally contributed to perform the experiment, as well as J.N., with help from D.C.G.; mlM.K. fabricated the sample on heterojunctions grown by I.F. and D.R.C.B. A.D., D.C.G. and P.R. analyzed and discussed the data. D.C.G. wrote the manuscript with inputs from all coauthors.

Competing interests

The authors declare no competing interests.

Additional information

Supplementary information The online version contains supplementary material available at https://doi.org/10.1038/s41467-025-63308-2.

Correspondence and requests for materials should be addressed to D. C. Glattli.

Peer review information *Nature Communications* thanks the anonymous reviewers for their contribution to the peer review of this work. A peer review file is available.